Resolvent Analysis of Large Aircraft Wings in Edge-of-the-Envelope Transonic Flow

Jelle Houtman* and Sebastian Timme†
University of Liverpool, Liverpool, L69 3GH, United Kingdom

Ati S Sharma‡
University of Southampton, Southampton, SO16 7QF, United Kingdom
Agalmic Ltd, Romsey, SO51 5SZ, United Kingdom

Shock-wave/boundary-layer interaction on wings can result first in self-sustained flow unsteadiness called shock buffet and eventually in a structural response called buffeting. While it is an important aspect of wing design and aircraft certification, particularly for modern transonic air transport, not all of the underlying multidisciplinary physics are thoroughly understood. Herein we focus the discussion on three main points. First, a practical implementation of an iterative resolvent method heavily relying on the efficient solution of large sparse linear systems of equations is introduced. Second, its application as a predictive tool to explore large scale flow unsteadiness on an aircraft wing early, following the work in Timme [1], is demonstrated. And third, we continue the exploration of the impact of the elastic wing structure in such flow conditions, following the work in Houtman and Timme [2]. An industrial computational fluid dynamics solver has previously been modified to solve the global stability problem that accounts for the aeroelastic coupling. Those ideas for linearised aerodynamics tools are expanded herein by a novel algorithm to address the now-ubiquitous resolvent problem aiming to compute optimal forcing and response when stability analysis alone is non-informative. The chosen test case is the NASA Common Research Model for which already both fluid modes on the rigid (yet statically deformed) wing and fluid-structure coupled modes on the corresponding elastic configuration are available as reference, helping guide the process. The results suggest that the resolvent approach is capable of predicting strong modal behaviour, such as linked to shock buffet, well before the notional onset of large scale unsteadiness when a global stability tool can first identify dominant coherent physics through weakly damped eigenmodes. On the question of including structural degrees-of-freedom in shock-buffet investigations, or not, it can be said that, while the coupled formulation can give a more complete picture of the physics overall (and is hence important to consider), in subcritical conditions the structual dynamics play a secondary role when optimally forcing the coupled system.

I. Introduction

Aeroelasticity is the field of engineering which aims to describe the deformation and motion of and fluid flow around objects, subject to aerodynamic, elastic and inertial forces, and has been studied for over a century [3–5]. Questions on fluid stability, in the absence of structural dynamics, have similarly been studied for decades [6]. By helping us elucidate phenomena that would otherwise remain a mystery, many objects that we use every day can be designed to be safer, faster and more efficient. Taking aeroplanes as a good example, many static and dynamic design challenges, such as torsional divergence, flutter, limit-cycle oscillation, shock buffet and structural buffeting, can have detrimental effects and lead to passenger discomfort, lowered system efficiency, structural fatigue and, in the worst case, complete destruction. Accurate (yet fast) methods to predict when these phenomena could happen, and how to prevent them, are therefore highly desirable in the industrial design iterations. Numerical analysis has proven a powerful tool in this regard, and invaluable insights have been gathered over the years.

One of those aforementioned phenomena, shock buffet, exhibits strong self-excited flow oscillations caused by the interaction of shock waves and the boundary layers forming over the aircraft wings in high-speed flight. Despite

*PhD Student, School of Engineering, jelle.houtman@liverpool.ac.uk.
†Senior Lecturer, School of Engineering, sebastian.timme@liverpool.ac.uk. Member AIAA.
‡Visitor, Engineering and Physical Sciences, a.sharma@soton.ac.uk

being first identified in the 1960s, a complete explanation incorporating the diverse inherent multidisciplinary aspects is still elusive, even though the body of experimental research continues to grow [7–9]. An acoustic feedback loop sustaining the shock oscillations was one of the first explanations given in [10], which has been corroborated by multiple experimental studies [8, 11]. On the other hand, numerous experimental and numerical studies have found spanwise outboard propagation of buffet cells, a distinct feature of shock buffet on finite wings. A major advancement came in the discovery of a global instability as a driver of aerofoil shock-buffet unsteadiness in [12], which led the way for similar findings on infinite-wing geometries, for which the impact of key geometric wing sizing parameters (such as aspect ratio and sweep angle) has been further explored [13–15]. Recently, practical finite-wing aircraft have been the subject of global stability studies [1, 16], with shock buffet being linked to a globally unstable mode, with successive studies aiming to understand the role of fluid-structure interaction on the same geometry [2, 17]. Independently, it has been shown for a pitch-plunge (and variants thereof) typical section aerofoil, that the introduction of an elastic structure has the ability to destabilise an otherwise stable flow in transonic conditions [18]. Global stability analysis involving fluid-structure interaction is indeed an active research area. Novel methods and physics, with unstable eigenmodes originating both in the fluid and the structural degrees-of-freedom, have been explored for various configurations, such as a cylinder with splitter plate, a spring-mounted plate and aerofoils [19–23]. Another important earlier study to be pointed out is that in [24] where the linearised physics were modelled in a similar approach to ours and applied to finite-wing flutter in inviscid flow.

Similarly, resolvent analysis has been used to further the understanding of flow physics. This method relies on the characteristics of the resolvent operator, instead of the direct linear Jacobian operator, which acts to transform an input (forcing) mode to an output (response) mode. The spectral properties of the resolvent operator can give insight to pseudo-resonance, as well as transient growth phenomena, due to the non-normality of the linear operator. Early work on this topic considered Poiseuille flow close to the laminar equilibrium, revealing that a laminar-turbulent transition was possible at subcritical flow conditions and that forcing even at frequencies away from the spectrum can give rise to large resonances [25, 26]. A similar analysis was later shown to apply to turbulent shear flows. In the turbulent case however, the forcing is endogenous to the flow, as the turbulent fluctuations drive themselves through the turbulent resolvent operator by nonlinear feedback [27]. In the turbulent analysis, the state is not assumed to be close to laminar equilibrium and the fluctuations are not required to be small. The resolvent (forcing and response) modes are calculated via the singular value decomposition of the resolvent of the Navier–Stokes operator formed about the turbulent mean. Such a study was also conducted for two-dimensional aerofoil shock buffet in [28], where resolvent analysis uncovered a secondary (pseudo-) resonance, separate from shock buffet found with a global stability analysis, and linked to a Kelvin–Helmholtz-type instability in the shear layer. Extending the idea to three-dimensional infinite wings, resolvent analysis proved to be an excellent tool to predict instabilities early on where global stability analysis is unsuccessful [29]. Herein, we formally introduce the therein employed iterative resolvent method, which is itself a modification of the method discussed in [30, 31]. In addition, we extend our resolvent tool to include fluid-structure interaction, similar to our previous global stability work [2], and use a sort of deflation approach to compute subsequent optimal modes corresponding to lower energy gains. An alternative route, in a fluid flow context, to enable resolvent analysis for more complex test cases was presented in [32]. The addition of a flexible structure in resolvent analysis has also been investigated for a two-dimensional boundary layer flow over a wall [33].

This work builds upon our previous efforts [2], where the aerodynamic shock-buffet instability on a large aircraft wing has been studied subject to aeroelastic coupling (following the work on the fluid-only system in [1, 29]). It was found that the coupling of fluid and structure destabilised modes that were otherwise stable in the fluid-only configuration and that the system could potentially be destabilised at lower angles of attack than what would be predicted without this coupling. Herein, the analysis is extended to investigate the resolvent operator when an elastic structure is included. This method requires modifications to the DLR–TAU solver that were first implemented for the eigenvalue problem encountered in global stability analysis, most importantly the application of the coupled preconditioner matrix in parallel, in order to use the resolvent method for large aircraft cases, relevant to industry. The energy gain, as well as the optimal forcing and response modes, are investigated to augment the previous eigenvalue studies to further elucidate the role of fluid-structure coupling on the otherwise purely aerodynamic shock-buffet phenomenon.

This document continues with a brief description of the physical models and implementation details in Section II. Here the focus is on the coupled Jacobian operator and the adaptation of the iterative resolvent method using a sparse iterative linear solver, implemented within the industrial DLR–TAU solver. The iterative resolvent method, which makes it possible to investigate practical aircraft test cases of arbitrary size, is explained for the first time. Finally, results for the NASA Common Research Model can be found in Section III, including a discussion on the steady base state, a reminder of our previous stability results [2], and the new resolvent results.

II. Theory and Methodology

A. Governing Equations of Fluid and Structure

The starting point of all our linearised analyses is the set of semi-discrete governing equations

$$\frac{\mathrm{d}\boldsymbol{w}}{\mathrm{d}t} = \boldsymbol{R}(\boldsymbol{w}) \tag{1}$$

The latter equation is used to describe both the aerodynamics and the multidisciplinary aeroelastic problem in a two-field formulation. For the aeroelastic analysis, the state vector $\boldsymbol{w}$ is split into two parts, $\boldsymbol{w} = [\boldsymbol{w}_f, \boldsymbol{w}_s]^T$, representing the fluid and structural degrees-of-freedom, respectively, and vector $\boldsymbol{R}$ contains the corresponding non-linear residual functions. The aerodynamic analysis discards the structural degrees-of-freedom. Clearly, eq. (1) depends on many independent parameters which are not explicitly stated herein for ease of notation.

The aerodynamics are assumed to be governed by the compressible Reynolds-averaged Navier–Stokes equations in three-dimensional space, coupled with a suitable model for turbulence closure, solving for the conservative variables of density ρ, three momentum components $\rho\boldsymbol{u}$ (with $\boldsymbol{u}$ containing the Cartesian velocity field), total energy ρE and the working variable $\rho\tilde{\nu}$ of the chosen turbulence model, specifically the negative Spalart–Allmaras model. The spatially discretised terms of the fluid model (with details to be provided in Section II.C) are contained in the residual vector $\boldsymbol{R}_f$, with its dimension given by the number of mesh points times conservative variables. The residual also contains the explicit dependence on the discrete cell volumes (resulting from a finite-volume formulation) and terms relating to deforming meshes in an arbitrary Lagrangian-Eulerian formulation, with details to be found e.g. in [34]. For the test cases of interest in our line of work, the structure is commonly described by a detailed finite-element model, which effectively discretises the second-order ordinary differential equation of a (damped) mass-spring system. A free vibration analysis gives a modal description of the aircraft structure (specifically normal mode shapes and structural frequencies). Using these spatial modes of vibration, the governing equations for the structural degrees-of-freedom are projected into the modal space, with its dimension according to the number of retained dominant modes (which is significantly lower than the number of both the fluid unknowns and the original structural degrees-of-freedom) and the modal structural degrees-of-freedom become the time-dependent modal amplitudes. In essence, the aircraft structure is described by a linear reduced-order model. Coupling between fluid and structure happens through (generalised) aerodynamic loads and structural deformations that deform the fluid mesh.

A more detailed description of the physics models used in this work has been presented previously and the interested reader is referred to that work [2].

B. Resolvent Method

With the governing equations of the fluid and structural systems defined, focus now shifts to the resolvent formulation where the paper's novel contribution lies (specifically the iterative solution approach to the resolvent problem). The unknowns of fluid and structure are decomposed into a turbulent time-average flow and static deformed state, respectively, and fluctuation vectors via $\boldsymbol{w}(\boldsymbol{x}, t) = \bar{\boldsymbol{w}}(\boldsymbol{x}) + \tilde{\boldsymbol{w}}(\boldsymbol{x}, t)$ which results in the linearised algebraic equations

$$\frac{\mathrm{d}\tilde{\boldsymbol{w}}}{\mathrm{d}t} = J\tilde{\boldsymbol{w}} + \tilde{\boldsymbol{f}} \tag{2}$$

where $J = \partial\boldsymbol{R}/\partial\boldsymbol{w}$ is a large sparse matrix either representing the fluid Jacobian matrix $J = J_{ff}$ or the coupled Jacobian matrix consisting of four blocks $J = [J_{ff}, J_{fs}; J_{sf}, J_{ss}]$. The vector $\tilde{\boldsymbol{f}} = \tilde{\boldsymbol{f}}(\boldsymbol{x}, t)$ is introduced as a time-dependent forcing, which can originate from external forcing and/or describe non-linear terms. The focus herein is on subcritical conditions which means in the framework of unsteady Reynolds-averaged Navier–Stokes modelling that the steady-state base flow is equal to the time-averaged mean flow and even in mildly supercritical flow this statement is still approximately true. There is also, of course, a debate on the meaning of turbulence modelling in linearised analyses in broader terms, and the mean flow calculation continues to rely on the assumption of a separation of scales [12, 35] between the large scale coherent structures, that can be integrated in time even with the chosen flow model, and the small spatial and temporal scales of turbulence accounted for by turbulence modelling and resulting eddy viscosity [36, 37].

Using orthogonality, eq. (2) is written at each separate angular frequency ω with $\tilde{\boldsymbol{w}}(\boldsymbol{x}, t) = \hat{\boldsymbol{w}}(\boldsymbol{x})e^{i\omega t}$ (and similarly for the forcing vector), such that,

$$i\omega\hat{\boldsymbol{w}} = J\hat{\boldsymbol{w}} + \hat{\boldsymbol{f}} \tag{3}$$

where $\hat{\boldsymbol{w}}$ and $\hat{\boldsymbol{f}}$ are the components of the response and forcing vector, respectively, at frequency ω. Rearranging leads to an input-output relation formulated by the resolvent operator R as

$$\hat{\boldsymbol{w}} = -R\hat{\boldsymbol{f}} \tag{4}$$

where R is explicitly given by $(J - i\omega I)^{-1}$. The resolvent operator can be thought of as transforming an (input) forcing vector $\hat{\boldsymbol{f}}$ into the (output) response state vector $\hat{\boldsymbol{w}}$ and is the focus of resolvent analysis. When the forcing is absent, eq. (3) becomes an eigenvalue problem for the linear operator J, discussed previously in [1, 2]. Resolvent analysis is concerned with investigating both the optimal forcing (and response) at a given frequency and also for which forcing frequency the largest responses are produced overall, thereby identifying strong modal behaviour.

For a given frequency ω, the maximum possible energy gain of the system, $G(\omega) = \sigma_1^2$, is expressed as

$$G(\omega) = \max_{\hat{f}} \frac{\langle \hat{\boldsymbol{w}}, \hat{\boldsymbol{w}} \rangle}{\langle \hat{\boldsymbol{f}}, \hat{\boldsymbol{f}} \rangle} = \max_{\hat{f}} \frac{\langle R^\dagger R\hat{\boldsymbol{f}}, \hat{\boldsymbol{f}} \rangle}{\langle \hat{\boldsymbol{f}}, \hat{\boldsymbol{f}} \rangle} \tag{5}$$

where $\langle \boldsymbol{a}, \boldsymbol{b} \rangle = \boldsymbol{a}^H Q \boldsymbol{b}$ defines the weighted inner product of two arbitrary vectors $\boldsymbol{a}$ and $\boldsymbol{b}$, with the matrix Q describing a suitable positive definite matrix, containing the discrete cell volumes on its diagonal in our case. Other inner products to define the energy gain have been discussed in the literature and can be explored in the future [38, 39]. The adjoint of the resolvent operator is $R^\dagger$, such that $\langle \boldsymbol{a}, R\boldsymbol{b} \rangle = \langle R^\dagger \boldsymbol{a}, \boldsymbol{b} \rangle$ or, more explicitly, $R^\dagger = Q^{-1} R^H Q = (Q^{-1} J^H Q + i\omega I)^{-1}$ (where $J^H = J^T$ and $J^\dagger = Q^{-1} J^H Q$). The optimal gain and its corresponding forcing and response modes are obtained by computing the singular value decomposition (SVD) of R, such that $R = U\Sigma V^H$, where Σ is a diagonal matrix containing the singular values σ_i (with $i = 1 \ldots n$ and n as the number of modes of interest) and U and V are unitary matrices, unitary with respect to Q (so that, for instance, $U^\dagger Q U = I$). In the case of resolvent analysis, the columns U_i and V_i can be interpreted as the response and forcing modes with corresponding singular values σ_i indicating the energy gain. Here, we are interested in the dominant modes of the SVD, having the largest singular values and therefore showing the largest amplification. Equivalently, eq. (5) can be treated as an eigenvalue problem for $RR^\dagger$ and $R^\dagger R$, which will give the forcing and response modes as their eigenvectors and the squared singular values as the eigenvalues. If the frequency shift $i\omega$ is equal to an eigenvalue of J, the resolvent operator becomes singular and the energy gain tends to infinity. In that case, the forcing and response mode become equal to the eigenvectors of $J^\dagger$ and J, respectively.

C. Numerical Approach

Aerostructural Analysis

The Reynolds-averaged Navier–Stokes equations (plus turbulence model) are solved using the industrial DLR–TAU code which uses a second-order, finite-volume, vertex-centred discretisation [40]. The inviscid fluxes are computed using a central scheme with matrix artificial dissipation. The Green–Gauss theorem is used to compute the gradients of flow variables for viscous fluxes and source terms. The far-field boundary is realised by the method of characteristics while the no-slip condition on viscous walls is enforced strongly. Additionally, when a symmetry plane boundary condition is required, this is imposed by removing components of the momentum equations normal to the plane. The turbulence closure is provided by the negative Spalart–Allmaras model using the Boussinesq eddy-viscosity assumption. A steady-state flow solution is calculated via the backward Euler method with lower-upper symmetric Gauss–Seidel iterations and local time-stepping. A geometric multi-grid method is also used to improve convergence rates.

The coupled aeroelastic problem requires solving the mass-spring-damper modal structural equations (with the modes shapes mapped one-to-one to the surface mesh for the fluid equations) with applied (generalised) aerodynamic forces iteratively in a staggered fashion updating the structural and fluid degrees-of-freedom in turn. While the Newmark-beta scheme can be used to integrate the structural equations in time, for the static coupling where the aerodynamic loads are balanced by the wing stiffness the structural degrees-of-freedom are updated iteratively based on the latest loads estimate. The coupling between aerodynamics and structure for these non-linear iterations (either for computing a base state or for unsteady time-stepping) is done using the tools provided through the FlowSimulator framework [41]. The fluid-structure coupling for linearised analyses in identifying and dealing with dominant modal behaviour (either global stability or resolvent) has been integrated entirely in the TAU flow solver [2].

First Discretise, Then Linearise Framework

The Jacobian matrix blocks of the linearisation are calculated on the statically deformed geometry for subsequent linearised aerodynamics analyses, specifically herein resolvent analysis. Matrices J_{ff} and J_{sf} are computed from a

Algorithm 1 Iterative resolvent method for n dominant modes

Require: Resolvent operator $R = (J - i\omega I)^{-1}$, convergence criterion c, number of modes n.

1: **for** $i = 1, ..., n$ **do**
2: Set a random initial forcing with $\langle \hat{\boldsymbol{f}}_i, \hat{\boldsymbol{f}}_i \rangle = 1$
3: **do**
4: $\hat{\boldsymbol{f}}_i = \hat{\boldsymbol{f}}_i - \sum_{j=1}^{i-1} \langle \hat{\boldsymbol{f}}_i, \hat{\boldsymbol{f}}_j \rangle \hat{\boldsymbol{f}}_j$
5: $\hat{\boldsymbol{f}}_{\text{old}} = \hat{\boldsymbol{f}}_i$
6: Solve $(J - i\omega I)\hat{\boldsymbol{u}}_i = \hat{\boldsymbol{f}}_i$ iteratively
7: $\sigma_i^2 = \langle \hat{\boldsymbol{u}}_i, \hat{\boldsymbol{u}}_i \rangle$ and $\hat{\boldsymbol{u}}_i = \hat{\boldsymbol{u}}_i / \sigma_i$
8: Solve $(J^\dagger + i\omega I)\hat{\boldsymbol{v}}_i = \hat{\boldsymbol{u}}_i$ iteratively
9: $\sigma_i^2 = \langle \hat{\boldsymbol{v}}_i, \hat{\boldsymbol{v}}_i \rangle$ and $\hat{\boldsymbol{f}}_i = \hat{\boldsymbol{v}}_i / \sigma_i$
10: **while** $\|\hat{\boldsymbol{f}}_i - \hat{\boldsymbol{f}}_{\text{old}}\| > c$
11: **end for**

hand-derived, analytical formulation, while J_{fs} is computed using a finite-difference method. Forming J_{ss} is trivial due to the modal nature of the structural system. Details on the meaning and simplifications can be found in [42].

Iterative Resolvent Method

Instead of directly computing the SVD of the resolvent operator R or the eigenvalue problems for $RR^\dagger$ and $R^\dagger R$, an iterative method is used. Conventional matrix-forming and/or direct methods are unsuitable due to the size of the linear operators that are required for the test cases of interest. Fortunately, we are interested in computing only a few of the leading modes with the largest energy gains. Therefore, we opt for an iterative method to compute the singular values (and corresponding vectors) of the resolvent operator. The iterative scheme is summarised in alg. 1. It is adapted from a similar time-stepping algorithm introduced in [30] and refined in [31]. The distinguishing feature is that we solve for the periodic state at the specified frequency directly, instead of time-stepping through multiple cycles until a periodic state is converged. By repeatedly applying the resolvent operator and its adjoint (cf. lines 6 and 8) and normalising the resulting vectors (cf. lines 7 and 9), the dominant response and forcing modes can be found iteratively with the energy gain given by their appropriate vector norm. Another feature is that deflation of converged optimal forcing modes (cf. line 4) allows the extraction of subsequent optimal modes with lower gains.

The iterative resolvent method involves applying the inverse of a linear operator to a vector, which in practice means the solution of a large sparse linear system of equations using an iterative solver due to the size of the operator. For solving either $R^{-1}\hat{\boldsymbol{u}} = (J - i\omega I)\hat{\boldsymbol{u}} = \hat{\boldsymbol{f}}$ or $R^{-\dagger}\hat{\boldsymbol{v}} = (J^\dagger + i\omega I)\hat{\boldsymbol{v}} = \hat{\boldsymbol{u}}$, we use a Krylov subspace method, in particular the generalised conjugate residual solver with inner orthogonalisation and deflated restarting (GCRO-DR) [43–45] with suitable preconditioning. The GCRO-DR solver aims to improve on the standard restarted generalized minimal residual method (GMRES) by recycling a suitable Krylov subspace between restarts (and in principle can also be used to recycle when solving for a sequence of linear system such as those arising from a changing right-hand side). This helps preventing the algorithm from stalling in particularly stiff cases and normally speeds up convergence. For preconditioning, we use a block-Jacobi preconditioner with block-local incomplete lower-upper (ILU) factorisation of the shifted fluid Jacobian matrix $(J_{ff} - i\omega I)$ for fluid-only cases and the so-called *arrowhead* preconditioner (making use of the aforementioned ILU factorisation for the fluid degrees-of-freedom) for the aeroelastic cases. This preconditioner, based on the inversion of block-arrowhead matrices shown in [46], allows the preconditioner matrix, which is an approximation of $(J - i\omega I)^{-1}$, to be applied in parallel for the coupled Jacobian matrix. Specifically, it includes the coupling matrices between fluid and structural degrees-of-freedom, resulting in a better approximation than would be obtained by, for instance, a block-Jacobi preconditioner which discards off-diagonal blocks. This idea was introduced in [2], where further details on the method can be found. Compared to a block-Jacobi preconditioner, significant speed-ups including the prevention of convergence stall were observed for the most challenging scenarios.

A representative convergence behaviour of the iterative method, using the full-span test case discussed in Section III, is shown in fig. 1. Before providing further explanations, it is stated that the lowest achievable level of convergence for the (outer) resolvent iteration depends on the chosen convergence tolerance of the (inner) iterative linear system solution. Herein, we initially adjusted the linear solver convergence tolerance based on the current level of outer convergence,

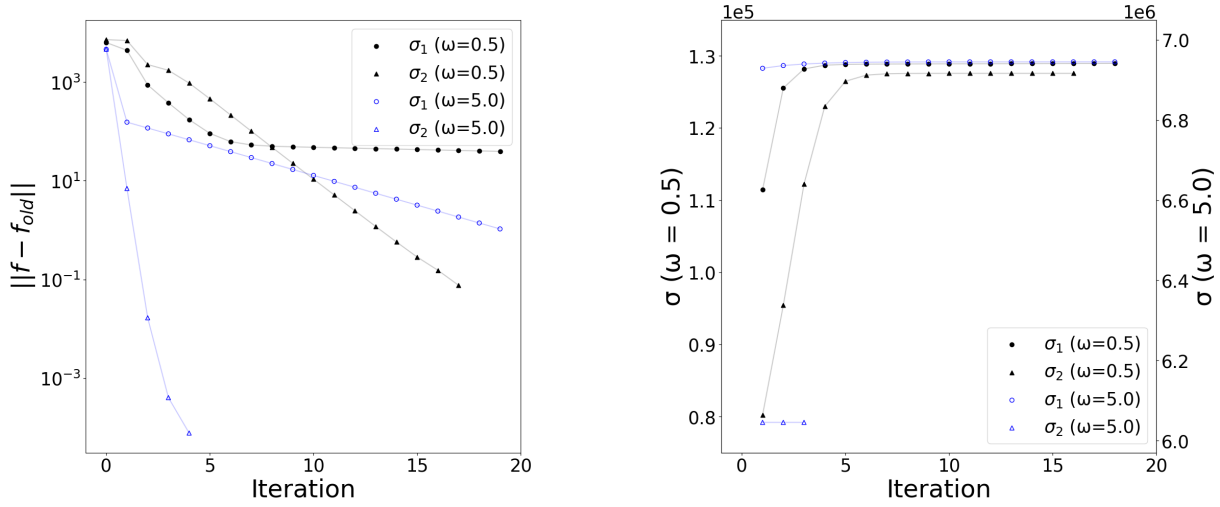

Fig. 1 Representative numerical behaviour of iterative resolvent method for full-span fluid-only calculations at angle of attack $\alpha = 3.5°$ and angular frequencies $\omega = 0.5$ and 5.0 showing the convergence of (left) the forcing vector through the Euclidean norm $\|f - f_{\text{old}}\|$ and (right) two leading singular values $\sigma_{1,2}$.

with a minimum capped at 10^{-7}. This can explain the floor of the trends shown in the figure. The figure demonstrates that well separated modes, such as the second optimal mode at $\omega = 5.0$ once the first optimal mode is deflated, converge rapidly. Hence, when strong modal behaviour is present in the system dynamics, the iterative resolvent method is very efficient. For modes that are harder to distinguish in their dominance, such as at $\omega = 0.5$, convergence can take significantly longer, while the singular values (shown in the right plot) are already sufficiently converged after a few iterations. For such scenarios, where for instance no clear winning mode is present or where pairs of modes can be found (such as a pair representing port/starboard wings), an Arnoldi method could be explored in future to enhance convergence rates [47]. Overall, the results agree nicely with the behaviour outlined in [31].

III. Results and Discussion

NASA Common Research Model Test Case

The NASA Common Research Model (CRM) resembles a modern passenger aeroplane and exists as both a physical model (for wind tunnel testing) and a computational model. It was designed as a universal test case for researchers to compare new ideas and results [48]. The wing has a nominal lift coefficient of 0.5, an aspect ratio of 9, a taper ratio of 0.275 and a 35° quarter-chord sweep angle. Herein, the scaled-down wind tunnel wing/body/horizontal-tail version is discussed featuring a mean aerodynamic chord of 0.189 m with a full span of 1.586 m and reference area of 0.280 m^2. The pylons and nacelles were discarded and the tail-setting angle was 0°. The computational mesh was generated for the half-span configuration with approximately 6.2×10^6 points including approximately 170 000 points on solid walls. A viscous wall normal spacing of $y^+ < 1$ is ensured. The hemispherical far-field boundary is located at a distance of 100 semi-span lengths. Mirroring with respect to the centre plan gives the full-span case. Modal shapes and structural frequencies were calculated from the finite-element model representing the wind-tunnel geometry*. The first 30 normal modes with lowest frequency are kept covering the shock-buffet frequency range previously identified. Further details, including a visualisation of representative mode shapes, can be found in [1, 2].

Herein, the Reynolds number (based on mean aerodynamic chord) is $Re = 5.0 \times 10^6$ and the free-stream Mach number is $M = 0.85$, chosen according to the test entry in the European Transonic Windtunnel [49]. The focus is on angles of attack giving subcritical flow conditions. Results are stated in their non-dimensional form throughout, based on the mean aerodynamic chord and reference free-stream values, unless explicitly specified otherwise. Full-span simulations with approximately 12.3×10^6 mesh points and nearly 74×10^6 complex-valued degrees-of-freedom are done on four compute nodes, each having twin Skylake 6138 processors, 40 hardware cores and 384 GB of memory.

*found at https://commonresearchmodel.larc.nasa.gov/

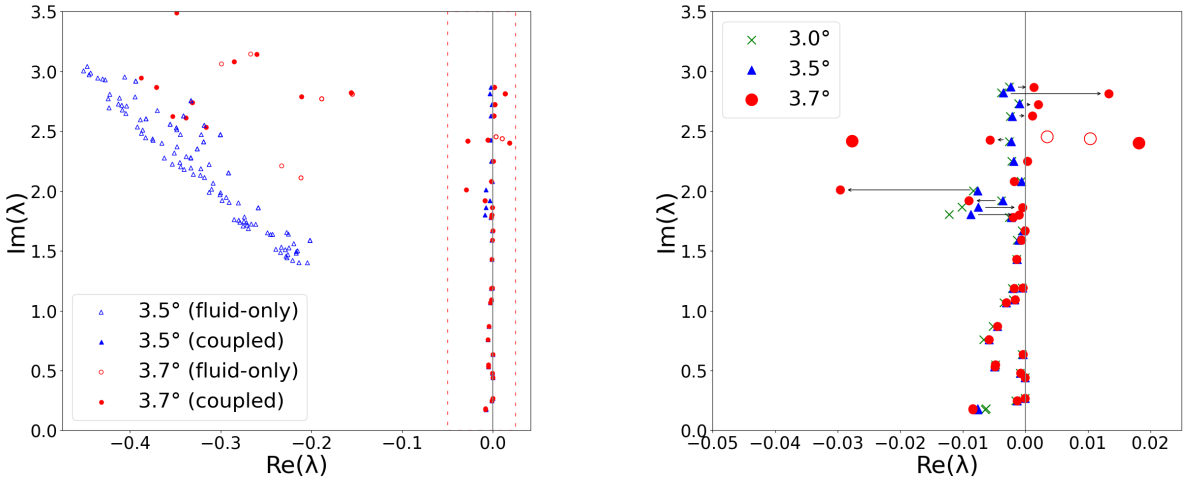

Fig. 2 Eigenvalues of fluid-only and coupled systems for angles of attack α = 3.0°, 3.5° and 3.7° showing (left) an overall view and (right) a zoomed-in region along the imaginary axis. The red box in the left plot indicates the region shown in the right plot.

Static Aeroelastic Base State

In preparation for using the resolvent method for the NASA CRM, the static aeroelastic deformation of the aircraft due to the aerodynamic loads is required. As described earlier, the structural and aerodynamic degrees-of-freedom are updated in turn. Altogether we specified 50 outer iterations of the fluid-structure coupled analysis, each with 100 iterations of the flow solver followed by loads transfer to the modal structural degrees-of-freedom, structural solution update and finally fluid mesh deformation. The coupled solutions used as base states for the subsequent linearised analyses, foremost for the calculation of the linear operator, converged at least by ten orders of magnitude. The resulting deformation of the geometry and surface pressure distribution for a representative angle of attack was shown previously in [2, 17] and agree well with equivalent measurements found experimentally in the European Transonic Windtunnel campaign [49]. Most importantly, an asymmetry between the port and starboard wing was highlighted, which is in contrast to the exact symmetry with respect to the fuselage centre plane discussed in [1] and is due to various cut-outs in the physical wind tunnel model needed for housing the instrumentation. Such detail was also included in the finite-element model and eventually propagates to the normal mode shapes and frequencies.

Stability Results

It is instructional when discussing pseudo-resonances in the resolvent results to be aware of weakly damped eigenmodes in the system dynamics as those can give rise to resonances. These were previously presented in [2] and are summarised for convenience in fig. 2. The figure shows global stability results, as growth rate Re(λ) over angular frequency Im(λ) with λ as the eigenvalue, at several angles of attack computed using both our implementation of the coupled eigenmode solver, presented in [2], and a conventional flutter analysis using unsteady aerodynamics based on computational fluid dynamics through the Schur complement method (pk-type flutter prediction), first presented in [50, 51]. The results are shown for the target conditions matching those in the wind tunnel. Focusing on angles of attack α = 3.5° and 3.7° several observations can be made. First, and obviously, results of the two available eigenmode solvers agree with the caveat that the conventional flutter method cannot pick up modes originating in the fluid degrees-of-freedom (hereafter called fluid modes). Hence, weakly damped fluid modes, eventually leading to large scale flow unsteadiness, require the coupled eigenmode solver. Also note, in [2] it was shown that the pk-type flutter tool can fail tracing eigenmodes originating in the structural degrees-of-freedom (hereafter called structural modes) in close proximity to fluid modes. Second, in the right plot, relatively little migration in the structural eigenvalues can be found going from angle of attack α = 3.0° to 3.5° throughout the frequency range and going from α = 3.5° to 3.7° for frequencies below those typically reported as characteristic frequency range for the shock-buffet on finite wings. Indeed, when fluid modes suggest globally unstable flow at α = 3.7°, structural modes show strong migration and several unstable modes are identified. Third, and most important for our discussion on using the resolvent method as a predictive tool to identify shock buffet early through pseudo-resonances, there are no weakly damped fluid modes in the

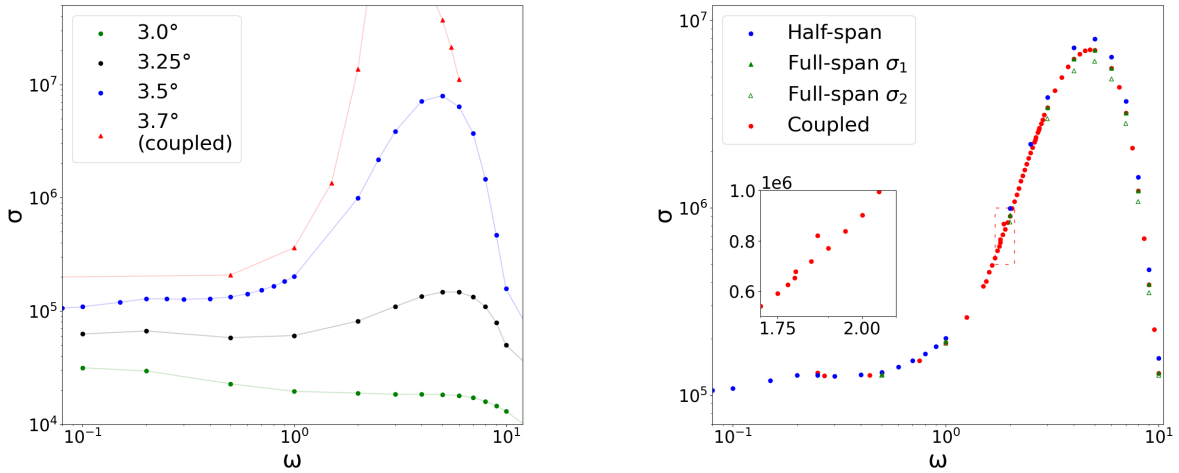

Fig. 3 Leading singular values $\sigma_1(\omega)$ showing (left) angles of attack α = 3.0°, 3.25° and 3.5° for half-span fluid-only case and α = 3.7° for fluid-structure coupled system and (right) focus angle of attack α = 3.5° with second largest singular value σ_2 included for full-span fluid-only case. The inset shows the region highlighted by the red box.

global stability results for angles of attack below $\alpha = 3.5°$, that can be distinguished from those spurious fluid modes associated with the numerical scheme rather than with dominant modal behaviour.

Resolvent Results

The iterative resolvent method was run for the fluid-only case at angles of attack $\alpha = 3.0°$, 3.25° (for the half-span configuration) and 3.5° (for both half- and full-span configuration) as well as for the fluid-structure coupled system at angles $\alpha = 3.5°$ and 3.7°. In addition, for the full-span fluid-only configuration, the two leading (optimal) modes were computed. All those thereby obtained singular values can be found in fig. 3. Several interesting observations can be made. First, in the left plot showing the angle-of-attack influence, while there is no strong peak to be found in the singular values at angles well below the critical value, the development of pronounced amplification due to optimal forcing tells the potential of the resolvent method as a predictive tool. Recall for instance, that for angles of attack $\alpha < 3.5°$, no weakly damped fluid modes can be found with the stability tool. Developing peaks in the energy gain can hence be explained by an increasing degree of non-normality in the system indicating pseudo-resonance. An increased angle of attack just above buffet onset in the fluid-structure coupled system at $\alpha = 3.7°$ results in a significant increase in energy gain, which has also been found in the two-dimensional aerofoil study in [28]. At this slightly supercritical angle of attack, the peak position in the gain has shifted from approximately $\omega = 5.0$ to a lower value of 2.5, which corresponds to the frequency of the leading fluid mode, seen in fig. 2. The almost two orders of magnitude higher singular value is now also a result of proper resonance in the proximity of the fluid mode. This statement can be explored more using the method outlined in [52]. Interpreting the optimal forcing of a globally unstable system should be done carefully; the use of the (statistically stationary) turbulent mean in the construction of J means that any exponential growth and saturation of disturbances associated with unstable eigenmodes has *already* taken place to form the assumed turbulent mean. As such, the response modes present in the flow are associated with purely oscillatory forcing. This means, unlike a classical linear modal stability analysis, it is the eigenvalues of J 'closest' to the imaginary axis that are shaping the flow structures, rather than the ones with the largest real part (see McKeon and Sharma [27] Appendix A). Second, the fluid-structure coupled system at angle of attack $\alpha = 3.5°$ in the right plot of fig. 3, with structural eigenmodes near the imaginary axis, shows a very similar amplification compared with the fluid-only case, suggesting, on the one hand, that the structural modes are not the cause of the peak and, on the other hand, that the effect of fluid-structure coupling on the dominant modal behaviour is not significant. Indeed, smaller secondary peaks in the frequency range $\omega = 1.5$ to 3.0, where we have chosen to refine the angular frequency spacing greatly, can be seen. The location of these peaks correspond to the frequencies of the structural eigenvalues found in fig. 2. Similar behaviour can also be seen in the verification of the iterative resolvent method in the appendix. However, these secondary peaks do not have a significantly higher gain than those in close vicinity, indicating that the effect of (pseudo-) resonance within

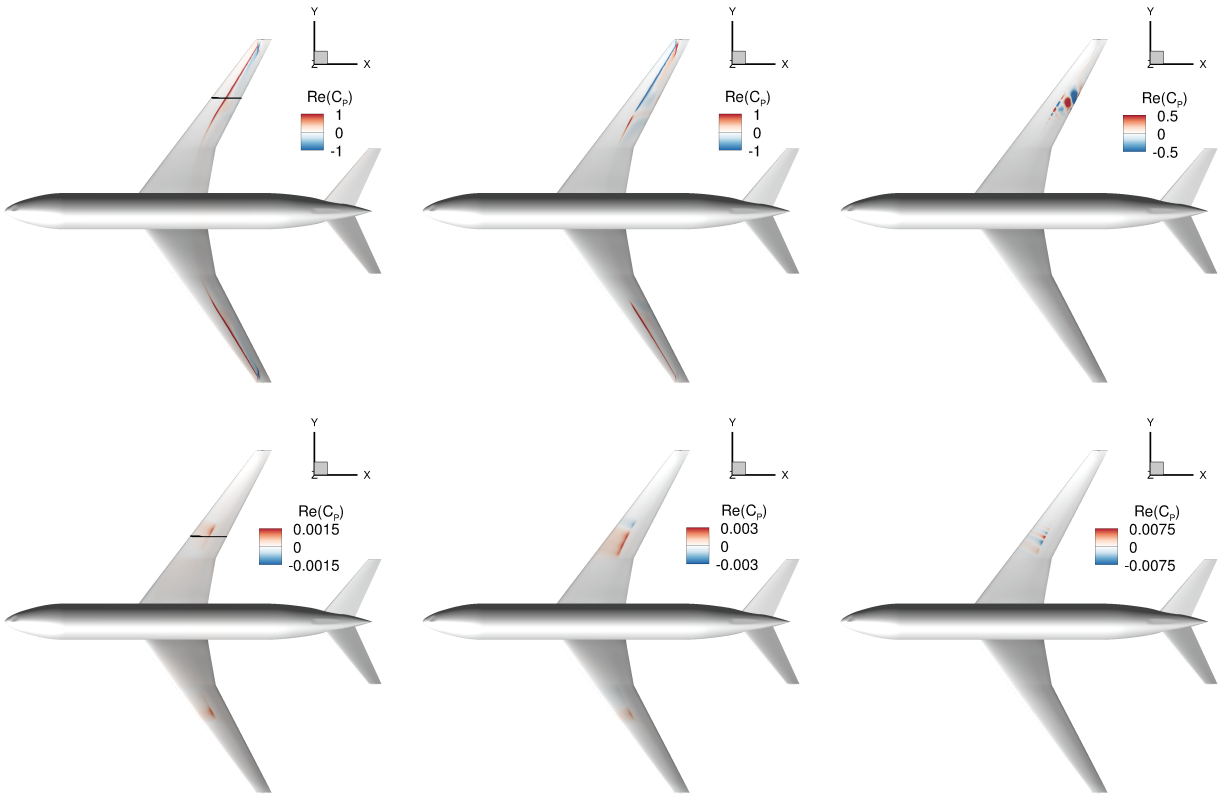

Fig. 4 Real part of perturbation in surface pressure coefficient of the response mode (top) and forcing mode (bottom) at angular frequencies $\omega = 0.25$ (left), 0.5 (middle), 5.0 (right) at angle of attack $\alpha = 3.5°$. The spanwise positions for the slices in fig. 5, specifically at non-dimensional span $\eta = 0.497$ and 0.66 for forcing and response modes, respectively, are shown as black lines.

the structural system is low compared to the non-normality of the fluid system. It will be instructive to explore this statement for instance at angle of attack $\alpha = 3.0°$ in the absence of a strong amplification arising from the fluid flow. Third, a smaller, yet noticeable peak can be found at very low frequencies at $\alpha = 3.5°$. This frequency range corresponds roughly to (quasi-) two-dimensional aerofoil modes found in previous studies [28, 29]. While we state this observation here to be comprehensive, additional simulations and scrutiny are required to reinforce the potential insight gained when also invoking the visualisations in figs. 4 and 5 which show response modes of very long wavelength in the order of a wing span and distinct features in the forcing modes. For instance, it will be valuable to compute the distance between the leading singular values in the figure and the next optimal modes; singular values identifying strong modal behaviour can be expected to be well separated (and hence relatively easy to converge) from lower ranked singular values. Lastly, the right plot shows the singular value of the second dominant modes for the full-span fluid-only case at angle of attack $\alpha = 3.50°$. While the theoretical and numerical properties of the iterative resolvent method dictate that the σ_2 values have to be lower than those of σ_1, they still show the characteristic broad peak. This is analogous to the behaviour of the eigenmodes when comparing the half- and full-span configurations in [2]. Specifically, due to the slight asymmetries in the finite-element structural model, there are pairs of weakly damped eigenmodes each emphasising the dynamics of one of the wings. Similarly, the forcing and response mode shapes, to be discussed next, show that these two leading optimal modes dominate one wing each (i.e. starboard and port wing for the first and second optimal modes, respectively).

Figures 4 and 5 offer a glimpse into the spatial characteristics of the first optimal forcing and response modes of the fluid-structure coupled system at angle of attack $\alpha = 3.5°$ and a few selected frequencies corresponding to distinct features discussed above. Note that, similar to the conclusion on the leading singular values in fig. 3, the fluid part of the forcing and response modes for the full-span fluid-only configuration is very similar and does thus not require special mentioning. In fig. 4, the forcing and response modes can be seen for the three angular frequencies $\omega = 0.25$, 0.5 and 5.0 showing the real part of the perturbation in the surface pressure coefficient. Starting with the highest

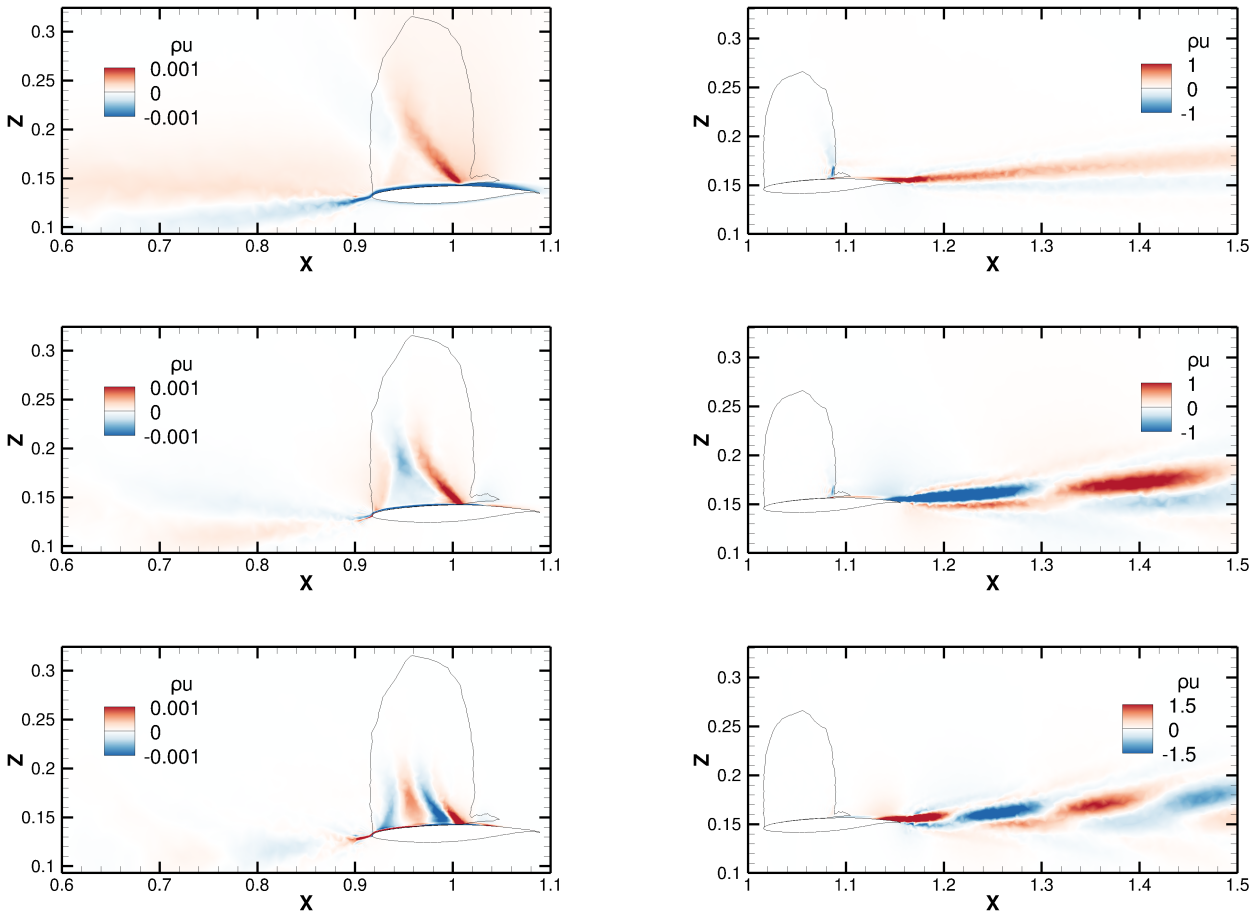

Fig. 5 Real part of x-momentum component $\widehat{\rho u}$ for forcing modes at non-dimensional span $\eta = 0.497$ (left column) and response modes at non-dimensional span $\eta = 0.66$ (right column) for non-dimensional frequencies $\omega = 0.5$ (top), 2.75 (middle) and 5.0 (bottom) and angle of attack $\alpha = 3.5°$. The sonic line is also shown.

frequency $\omega = 5.0$, which corresponds to the peak in the energy gain at this angle of attack, the response mode reveals a strong resemblance to the finite-wing shock-buffet modes with so-called buffet cells visible aft of the shock front on the starboard wing [1, 2]. Observe that the second optimal mode gives similar spatial structures on the port wing instead. Equally, the forcing mode shape comes with features resembling the adjoint shock-buffet mode visualised in [53]. Hence, the major peak discussed in the narrative relating to fig. 3 can indeed be regarded as an early indicator (at lower angles of attack) of imminent global aerodynamic instability, even though no weakly damped and distinguishable eigenmodes can be found. Furthermore, analysing the phase, specifically $\angle\hat{C}_P = \arctan(\mathrm{Im}(\hat{C}_P)/\mathrm{Re}(\hat{C}_P))$, this mode is shown to be outboard running, again similar to the global unstable shock-buffet mode. Note that similar statements can be made for the modes at the other frequencies constituting the peak and these are not explicitly shown herein. For instance, at angular frequency $\omega = 2.75$, which is close to the frequency of the leading eigenmode at the instability onset angle of attack, similar but coarser-grained features (effectively correlated with the forcing frequency) can be identified, as indicated in fig. 5 (middle row) through the real part of the streamwise momentum component.

The discussion now turns to the far more subtle peak in fig. 3 at lower frequency. Inspecting the response mode visualisation in fig. 4, it becomes clear immediately that, in contrast to the higher frequency $\omega = 5.0$, the lower frequencies show perturbation amplitudes on both wings, which could indicate that this dominant mode is different in nature. It is similarly interesting to observe that the forcing on the wing surface is rather localised compared with the significant span extent of the response mode in the order of a wing (semi-) span. In this context it is also important to mention the long wavelength modes discussed in [54] (using modal decomposition of scale-resolved numerical

simulation data) and [55] (using modal decomposition of experimental dynamic pressure sensitive paint data). In those papers there is discussion on the direction of the spanwise modes, either inboard or outboard, and we find an outboard propagation direction which agrees with the 80%-scaled CRM wing study in [54], albeit that study being in an established shock-buffet condition. Returning to the forcing mode and inspecting a slice shown in fig. 5, a striking resemblance with the adjoint eigenmode near the shock-buffet onset angle of attack on both a two-dimensional aerofoil [28] and a three-dimensional infinite wing [29] can be noted. Of course, herein we are dealing with a three-dimensional finite wing and hence variation in the span direction must be taken into account. A prominent feature is the oblique line impacting in the region where the boundary layer separates. It was demonstrated that this oblique part of the forcing mode coincides with a right characteristic line, emphasising the importance to the whole dynamics of the shock-wave/boundary layer interaction. The reader is referred to [28] for more discussion on this point. As stated earlier, more scrutiny concerning these findings is required going forward, as is a more thorough discussion on the structural degrees-of-freedom in the fluid-structure coupled results. We conclude by pointing out, and explaining the reasoning behind, the different angular frequencies presented in figs. 4 and 5. Essentially, the spatial structures as presented in the plots will change gradually as the frequency is varied, and the results we selected provide an excellent picture of the forcing and response modes.

IV. Conclusion

Continuing from previous global stability studies, resolvent analysis is discussed to further elucidate the modal nature of the shock-buffet phenomenon on finite wings. The size and complexity of the target application, specifically large aircraft wings, and resulting big fluid meshes rule out the use of direct matrix-forming solution methods. Instead, by approximating the underlying singular value decomposition of the resolvent operator, a measure can be given to the optimal energy increase at a given frequency. This approximation is accomplished through an iterative method, presented here for the first time, implemented in the industrial DLR–TAU solver, and expanded to include structural degrees-of-freedom for aeroelastic analysis. The iterative method relies on the robust solution of large sparse linear systems of equations achieved through using an advanced preconditioned Krylov subspace iterative solver. By harmonically forcing an otherwise globally stable (or marginally unstable) system herein, the optimal energy gain can be computed, alongside the respective forcing and response modes. Deflation of converged optimal forcing modes, gives access to additional optimal modes which is useful when multiple dominant modes are present.

The NASA Common Research Model served as the test case, considering both a rigid (yet statically deformed) and an elastic configuration, at a free-stream Mach number of 0.85 and a chord Reynolds number of 5×10^6 according to an experimental test entry. The rigid case describes a fluid-only aerodynamic problem, that is discussed at three angles of attack below the onset of large scale unsteadiness. The resolvent approach is shown to be capable of predicting strong modal behaviour, such as linked to shock buffet on a finite wing, well before the notional onset of large scale unsteadiness when a global stability tool can first identify dominant coherent physics through weakly damped eigenmodes. Approximately half a degree below the critical angle of attack, a broadband pseudo-resonance peak is picked up through optimally forcing the system. The spatial structures of the corresponding forcing and response modes show clear similarities with those of the adjoint and direct eigenmodes, respectively, found through global stability analysis at angles of attack closer to critical conditions. On the question of including structural degrees-of-freedom in shock-buffet investigations, or not, it can be said that, while the coupled formulation can give a more complete picture of the physics overall (and is hence important to consider as we have previously argued in [2]), in subcritical conditions the structural dynamics play a secondary role when optimally forcing the coupled aeroelastic system. Finally, while it requires more simulations and scrutiny, the current results also indicate a weaker modal behaviour at frequencies which are typically described to be linked to an aerofoil-type mode, i.e. with a very long wavelength of the order of a wing span. Such modal nature was not previously identified through global stability analysis on the finite swept wing.

Appendix

Different test cases have been considered while implementing and verifying the methods discussed in this paper. In the following, we provide some detail of the flow over the widely used circular cylinder at a subcritical Reynolds number (for the fluid-only resolvent formulation) and the aeroelastic Goland wing (for the fluid-structure formulation).

A. Circular Cylinder

The laminar cylinder flow is discussed at a Reynolds number of $Re = 40$ (and low Mach number of $M = 0.2$). For demonstration purposes, a rather coarse mesh with just under 10 000 points is used with the domain extending to a

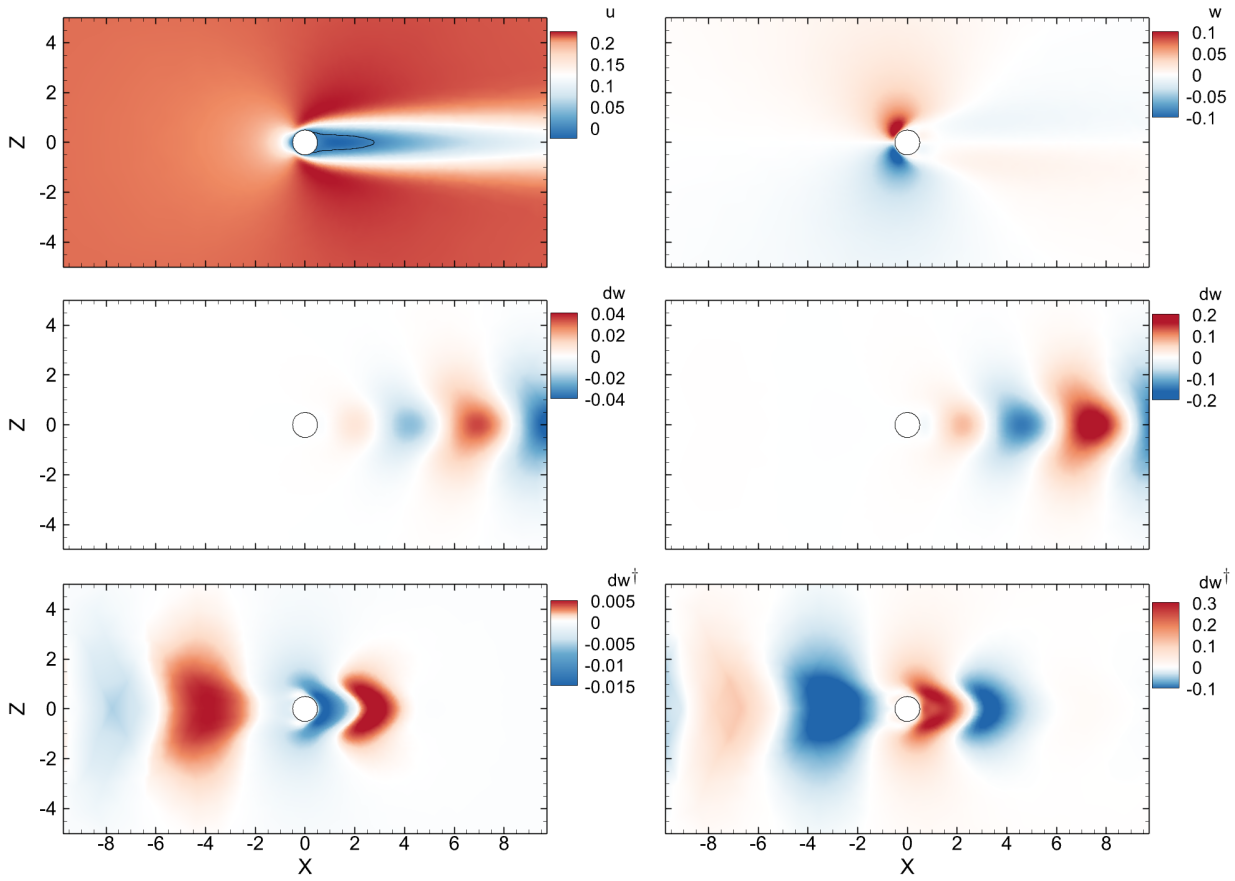

Fig. 6 Circular cylinder test case showing (top row) base-flow streamwise and cross-stream velocity components, (middle row) real part of cross-stream velocity component of the leading direct eigenmode (left column) and optimal response mode (right column), and (bottom row) real part of cross-stream velocity component of the leading adjoint eigenmode (left column) and optimal forcing mode (right column).

farfield boundary of 100 cylinder diameters. The convergence tolerance is set to 10^{-12} throughout both for non-linear iterations of the state-steady computation and the linear systems arising from the linearised aerodynamics methods. The base flow as steady solution of the Navier–Stokes equations is given in the top row of fig. 6 showing streamwise and cross-stream velocity components. Stability analysis (both the direct/right and adjoint/left calculation) predicts the leading mode (least damped) with an eigenvalue of $\lambda = -0.0275 + i0.7145$, which eventually develops into the vortex shedding instability at the critical Reynolds number of approximately $Re = 47 - 48$. The corresponding eigenfunctions of the cross-stream velocity component are shown in the left column in the figure, specifically the direct mode in the middle row (denoted dw) and the adjoint mode in the bottom row (denoted d$w^\dagger$). The eigenvectors are scaled to unit length. Results are consistent with published results in the literature [56, 57]. The resolvent analysis is done for a frequency $\omega = 0.7$ and the first three optimal modes are computed. The three largest singular values of those modes are $\sigma_1 = 2158.98$, $\sigma_2 = 162.66$ and $\sigma_3 = 153.75$. For debugging purposes these calculations were also done using Matlab functions to compute the largest eigenvalues of $RR^\dagger$ as well as the iterative method, described in alg. 1. The TAU implementation gives identical results while also testing parallel processing on different numbers of cores. The first optimal forcing and response modes are shown in the right column of the figure. The resemblance but not perfect agreement with the eigenmodes is expected [52]. Note that no effort was made to scale the different modes.

B. Goland Wing

The Goland wing is introduced for debugging purposes of the fluid-structure coupled implementation. This wing is cantilevered with a 4% thick parabolic arc aerofoil and a (semi-) span of 20 ft and chord length of 6 ft. The structure is

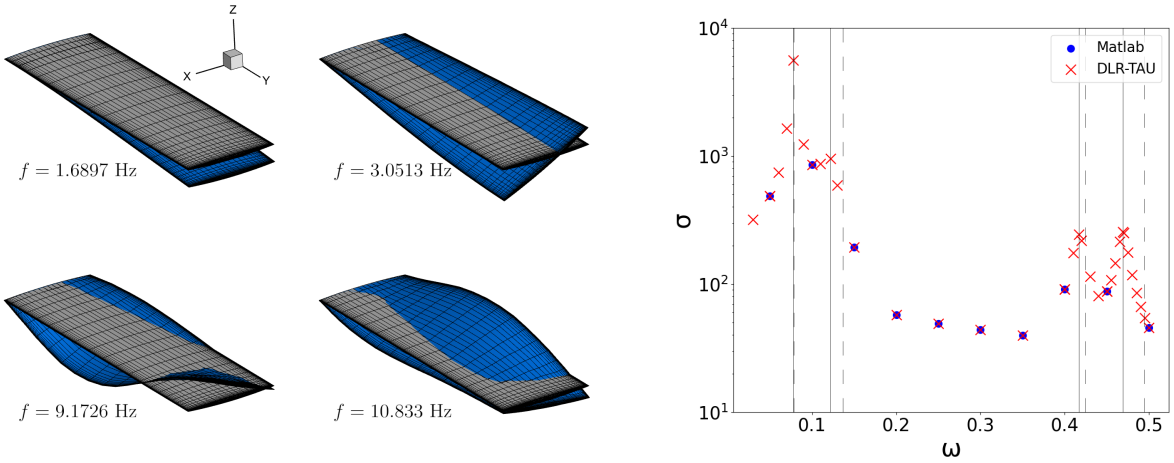

Fig. 7 Details of Goland wing test case showing (left) structural vibration mode shapes (in blue) and frequencies and (right) first singular value σ over forcing frequency ω. Dashed and solid vertical lines in the right plot correspond to the wind-off (as given in the left plot) and wind-on structural frequencies, respectively.

modelled by a finite-element method with details to be found in [58]. While we show results for a rather coarse fluid mesh with 17 268 points herein, a significantly finer mesh has been discussed previously as well [2]. A symmetry boundary condition is imposed at the wing-root plane. Inviscid flow at a reference free-stream Mach number of $M = 0.845$ and zero degree angle of attack is assumed. The target altitude (to establish air density and velocity according to the standard atmosphere) for the aeroelastic analysis is 30 000 ft. Figure 7 shows both the wing surface deformations according to the first four dominant structural modes of vibration and corresponding frequencies and the resolvent results. The first singular value was initially computed for eleven frequencies ranging from $\omega = 0.0$ to 0.5 in steps of $\Delta\omega = 0.05$ using the iterative method implemented in both the TAU code and Matlab (based on the matrices exported from the flow solver enhanced with aeroelastic functionality). The results as presented in the right plot are identical further supporting the notion of a correct TAU implementation. Following this reassurance, a good number of additional frequencies were considered to identify the peaks corresponding to the aeroelastic modes identifiable from a flutter analysis, as demonstrated in [2], clearly. Specifically, the eigenvalue around $\omega = 0.08$ lies closest to the forcing frequency, which corresponds to the largest singular value. In this simple high-subsonic inviscid test case without shock waves or shock-wave/boundary-layer interaction, strong amplification gains due to non-normality in the governing equations, specifically the Euler equations, are not expected.

Acknowledgments

The first author is grateful for support by an Engineering and Physical Sciences Research Council (EPSRC) Industrial CASE scholarship in partnership with Airbus. We also happily acknowledge financial support by the EPSRC through the joint grant EP/R037027/1 and EP/R037167/1. Last but not least, we thank the University of Liverpool for computing time on the high-performance computing system and both the German Aerospace Center (DLR) and Airbus for access to the TAU flow solver and FlowSimulator tools (for static aeroelastic coupling).

References

[1] Timme, S., "Global instability of wing shock-buffet onset," *Journal of Fluid Mechanics*, Vol. 885, 2020, p. A37. https://doi.org/10.1017/jfm.2019.1001.

[2] Houtman, J., and Timme, S., "Towards Global Stability Analysis of Flexible Aircraft in Edge-of-the-Envelope Flow," *AIAA Scitech 2021 Forum*, 2021. https://doi.org/10.2514/6.2021-0610.

[3] Livne, E., "Future of Airplane Aeroelasticity," *Journal of Aircraft*, Vol. 40, No. 6, 2003, pp. 1066–1092. https://doi.org/10.2514/2.7218.

[4] Shubov, M. A., "Flutter Phenomenon in Aeroelasticity and Its Mathematical Analysis," *Journal of Aerospace Engineering*, Vol. 19, No. 1, 2006, pp. 1–12. https://doi.org/10.1061/(ASCE)0893-1321(2006)19:1(1).

[5] Beran, P., Stanford, B., and Schrock, C., "Uncertainty Quantification in Aeroelasticity," *Annual Review of Fluid Mechanics*, Vol. 49, No. 1, 2017, pp. 361–386. https://doi.org/10.1146/annurev-fluid-122414-034441.

[6] Theofilis, V., "Global Linear Instability," *Annual Review of Fluid Mechanics*, Vol. 43, No. 1, 2011, pp. 319–352. https://doi.org/10.1146/annurev-fluid-122109-160705.

[7] Tijdeman, H., "Investigations of the transonic flow around oscillating airfoils," Tech. Rep. NLR-TR 77090 U, Nationaal Lucht-en Ruimtevaartlaboratorium, 1977. URL http://resolver.tudelft.nl/uuid:b07421b9-136d-494c-a161-b188e5ba1d0d.

[8] Jacquin, L., Molton, P., Deck, S., Maury, B., and Soulevant, D., "Experimental Study of Shock Oscillation over a Transonic Supercritical Profile," *AIAA Journal*, Vol. 47, No. 9, 2009, pp. 1985–1994. https://doi.org/10.2514/1.30190.

[9] Dandois, J., "Experimental study of transonic buffet phenomenon on a 3D swept wing," *Physics of Fluids*, Vol. 28, No. 1, 2016, 016101. https://doi.org/10.1063/1.4937426.

[10] Lee, B. H. K., "Oscillatory shock motion caused by transonic shock boundary-layer interaction," *AIAA Journal*, Vol. 28, No. 5, 1990, pp. 942–944. https://doi.org/10.2514/3.25144.

[11] Feldhusen-Hoffmann, A., Statnikov, V., Klaas, M., and Schröder, W., "Investigation of shock-acoustic-wave interaction in transonic flow," *Experiments in Fluids*, Vol. 59, No. 1, 2018, 15. https://doi.org/10.1007/s00348-017-2466-z.

[12] Crouch, J. D., Garbaruk, A., Magidov, D., and Travin, A., "Origin of transonic buffet on aerofoils," *Journal of Fluid Mechanics*, Vol. 628, 2009, p. 357–369. https://doi.org/10.1017/S0022112009006673.

[13] Paladini, E., Beneddine, S., Dandois, J., Sipp, D., and Robinet, J.-C., "Transonic buffet instability: From two-dimensional airfoils to three-dimensional swept wings," *Physical Review Fluids*, Vol. 4, 2019, p. 103906. https://doi.org/10.1103/PhysRevFluids.4.103906.

[14] Crouch, J. D., Garbaruk, A., and Strelets, M., "Global instability in the onset of transonic-wing buffet," *Journal of Fluid Mechanics*, Vol. 881, 2019, p. 3–22. https://doi.org/10.1017/jfm.2019.748.

[15] He, W., and Timme, S., "Triglobal infinite-wing shock-buffet study," *Journal of Fluid Mechanics*, Vol. 925, 2021, p. A27. https://doi.org/10.1017/jfm.2021.678.

[16] Timme, S., and Thormann, R., "Towards three-dimensional global stability analysis of transonic shock buffet," *AIAA Atmospheric Flight Mechanics Conference*, 2016. https://doi.org/10.2514/6.2016-3848, AIAA 2016-3848.

[17] Belesiotis-Kataras, P., and Timme, S., "Aeroelastic Coupling Effects in Globally Unstable Transonic Wing Flow," *AIAA Scitech 2021 Forum*, 2021. https://doi.org/10.2514/6.2021-0611.

[18] Nitzsche, J., Ringel, L. M., Kaiser, C., and Hennings, H., "Fluid-mode flutter in plane transonic flows," *IFASD 2019 – International Forum on Aeroelasticity and Structural Dynamics*, 2019. URL https://elib.dlr.de/127989/.

[19] Pfister, J.-L., Marquet, O., and Carini, M., "Linear stability analysis of strongly coupled fluid–structure problems with the Arbitrary-Lagrangian–Eulerian method," *Computer Methods in Applied Mechanics and Engineering*, Vol. 355, 2019, pp. 663–689. https://doi.org/https://doi.org/10.1016/j.cma.2019.06.024.

[20] Pfister, J.-L., and Marquet, O., "Fluid–structure stability analyses and nonlinear dynamics of flexible splitter plates interacting with a circular cylinder flow," *Journal of Fluid Mechanics*, Vol. 896, 2020.

[21] Negi, P. S., Hanifi, A., and Henningson, D. S., "On the linear global stability analysis of rigid-body motion fluid–structure-interaction problems," *Journal of Fluid Mechanics*, Vol. 903, 2020.

[22] Negi, P. S., Hanifi, A., and Henningson, D. S., "Linearized Formulation for Fluid-Structure-Interaction for Rigid-Body Motion," *IUTAM Laminar-Turbulent Transition*, Springer, 2022, pp. 459–468.

[23] Moulin, J., and Marquet, O., "Flow-induced instabilities of springs-mounted plates in viscous flows: A global stability approach," *Physics of Fluids*, Vol. 33, No. 3, 2021, p. 034133.

[24] Lesoinne, M., Sarkis, M., Hetmaniuk, U., and Farhat, C., "A linearized method for the frequency analysis of three-dimensional fluid/structure interaction problems in all flow regimes," *Computer Methods in Applied Mechanics and Engineering*, Vol. 190, No. 24, 2001, pp. 3121–3146. https://doi.org/https://doi.org/10.1016/S0045-7825(00)00385-6, advances in Computational Methods for Fluid-Structure Interaction.

[25] Trefethen, L. N., Trefethen, A. E., Reddy, S. C., and Driscoll, T. A., "Hydrodynamic Stability Without Eigenvalues," *Science*, Vol. 261, No. 5121, 1993, pp. 578–584. https://doi.org/10.1126/science.261.5121.578.

[26] Jovanovic, M., and Bamieh, B., "Componentwise Energy Amplification in Channel Flows," *Journal of Fluid Mechanics*, Vol. 534, 2005, pp. 145–183. https://doi.org/10.1017/S0022112005004295.

[27] McKeon, B. J., and Sharma, A. S., "A critical-layer framework for turbulent pipe flow," *Journal of Fluid Mechanics*, Vol. 658, 2010, p. 336–382. https://doi.org/10.1017/S002211201000176X.

[28] Sartor, F., Mettot, C., and Sipp, D., "Stability, receptivity, and sensitivity analyses of buffeting transonic flow over a profile," *AIAA Journal*, Vol. 53, No. 7, 2015, pp. 1980–1993. https://doi.org/10.2514/1.J053588.

[29] He, W., and Timme, S., "Resolvent Analysis of Shock Buffet on Infinite Wings," *AIAA Aviation 2020 Forum*, 2020. https://doi.org/10.2514/6.2020-2727.

[30] Monokrousos, A., Åkervik, E., Brandt, L., and Henningson, D. S., "Global three-dimensional optimal disturbances in the Blasius boundary-layer flow using time-steppers," *Journal of Fluid Mechanics*, Vol. 650, 2010, pp. 181—-214. https://doi.org/10.1017/S0022112009993703.

[31] Gómez, F., Sharma, A. S., and Blackburn, H. M., "Estimation of unsteady aerodynamic forces using pointwise velocity data," *Journal of Fluid Mechanics*, Vol. 804, 2016, p. R4. https://doi.org/10.1017/jfm.2016.546.

[32] Ribeiro, J. H. M., Yeh, C.-A., and Taira, K., "Randomized resolvent analysis," *Phys. Rev. Fluids*, Vol. 5, 2020, p. 033902. https://doi.org/10.1103/PhysRevFluids.5.033902.

[33] Pfister, J.-L., Fabbiane, N., and Marquet, O., "Resolvent analysis of boundary-layer flows interacting with finite-extent visco-elastic insert," *ICTAM 2021*, Milan (Virtuel), France, 2021. URL https://hal.archives-ouvertes.fr/hal-03368404.

[34] Thormann, R., and Widhalm, M., "Linear-Frequency-Domain Predictions of Dynamic-Response Data for Viscous Transonic Flows," *AIAA Journal*, Vol. 51, No. 11, 2013, pp. 2540–2557. https://doi.org/10.2514/1.J051896.

[35] Sipp, D., Marquet, O., Meliga, P., and Barbagallo, A., "Dynamics and Control of Global Instabilities in Open-Flows: A Linearized Approach," *Applied Mechanics Reviews*, Vol. 63, No. 3, 2010. https://doi.org/10.1115/1.4001478.

[36] Reynolds, W. C., and Hussain, A. K. M. F., "The mechanics of an organized wave in turbulent shear flow. Part 3. Theoretical models and comparisons with experiments," *Journal of Fluid Mechanics*, Vol. 54, No. 2, 1972, p. 263–288. https://doi.org/10.1017/S0022112072000679.

[37] Mettot, C., Sipp, D., and BÃ©zard, H., "Quasi-laminar stability and sensitivity analyses for turbulent flows: Prediction of low-frequency unsteadiness and passive control," *Physics of Fluids*, Vol. 26, No. 4, 2014, p. 045112. https://doi.org/10.1063/1.4872225.

[38] Yeh, C.-A., and Taira, K., "Resolvent-analysis-based design of airfoil separation control," *Journal of Fluid Mechanics*, Vol. 867, 2019, p. 572–610. https://doi.org/10.1017/jfm.2019.163.

[39] Bonne, N., Brion, V., Garnier, E., Bur, R., Molton, P., Sipp, D., and Jacquin, L., "Analysis of the two-dimensional dynamics of a Mach 1.6 shock wave/transitional boundary layer interaction using a RANS based resolvent approach," *Journal of Fluid Mechanics*, Vol. 862, 2019, p. 1166–1202. https://doi.org/10.1017/jfm.2018.932.

[40] Schwamborn, D., Gerhold, T., and Heinrich, R., "The DLR TAU-code: Recent applications in research and industry," *ECCOMAS CFD 2006: Proceedings of the European Conference on Computational Fluid Dynamics*, 2006.

[41] Reimer, L., Heinrich, R., and Ritter, M., "Towards Higher-Precision Maneuver and Gust Loads Computations of Aircraft: Status of Related Features in the CFD-Based Multidisciplinary Simulation Environment FlowSimulator," *New Results in Numerical and Experimental Fluid Mechanics XII*, edited by A. Dillmann, G. Heller, E. Krämer, C. Wagner, C. Tropea, and S. Jakirlić, Springer International Publishing, Cham, 2020, pp. 597–607. https://doi.org/10.1007/978-3-030-25253-3_57.

[42] Badcock, K., Timme, S., Marques, S., Khodaparast, H., Prandina, M., Mottershead, J., Swift, A., Ronch], A. D., and Woodgate, M., "Transonic aeroelastic simulation for instability searches and uncertainty analysis," *Progress in Aerospace Sciences*, Vol. 47, No. 5, 2011, pp. 392 – 423. https://doi.org/10.1016/j.paerosci.2011.05.002.

[43] Parks, M. L., de Sturler, E., Mackey, G., Johnson, D. D., and Maiti, S., "Recycling Krylov Subspaces for Sequences of Linear Systems," *SIAM Journal on Scientific Computing*, Vol. 28, No. 5, 2006, pp. 1651–1674. https://doi.org/10.1137/040607277.

[44] Niu, Q., Lu, L.-Z., and Liu, G., "Accelerated GCRO-DR method for solving sequences of systems of linear equations," *Journal of Computational and Applied Mathematics*, Vol. 253, 2013, pp. 131 – 141. https://doi.org/https://doi.org/10.1016/j.cam.2013.04.013.

[45] Xu, S., and Timme, S., "Robust and efficient adjoint solver for complex flow conditions," *Computers & Fluids*, Vol. 148, 2017, pp. 26 – 38. https://doi.org/10.1016/j.compfluid.2017.02.012.

[46] Stanimirović, P. S., Katsikis, V. N., and Kolundžija, D., "Inversion and pseudoinversion of block arrowhead matrices," *Applied Mathematics and Computation*, Vol. 341, 2019, pp. 379 – 401. https://doi.org/10.1016/j.amc.2018.09.006.

[47] Barkley, D., Blackburn, H. M., and Sherwin, S. J., "Direct optimal growth analysis for timesteppers," *International Journal for Numerical Methods in Fluids*, Vol. 57, No. 9, 2008, pp. 1435–1458. https://doi.org/https://doi.org/10.1002/fld.1824.

[48] Vassberg, J., Dehaan, M., Rivers, M., and Wahls, R., "Development of a Common Research Model for Applied CFD Validation Studies," *26th AIAA Applied Aerodynamics Conference*, 2008. https://doi.org/10.2514/6.2008-6919.

[49] Lutz, T., Gansel, P. P., Waldmann, A., Zimmermann, D.-M., and Schulte am Hülse, S., "Prediction and Measurement of the Common Research Model Wake at Stall Conditions," *Journal of Aircraft*, Vol. 53, No. 2, 2016, pp. 501–514. https://doi.org/10.2514/1.C033351.

[50] Timme, S., Marques, S., and Badcock, K. J., "Transonic Aeroelastic Stability Analysis Using a Kriging-Based Schur Complement Formulation," *AIAA Journal*, Vol. 49, No. 6, 2011, pp. 1202–1213. https://doi.org/10.2514/1.J050975.

[51] Bekemeyer, P., and Timme, S., "Flexible aircraft gust encounter simulation using subspace projection model reduction," *Aerospace Science and Technology*, Vol. 86, 2019, pp. 805 – 817. https://doi.org/10.1016/j.ast.2019.02.011.

[52] Symon, S., Rosenberg, K., Dawson, S. T. M., and McKeon, B. J., "Non-normality and classification of amplification mechanisms in stability and resolvent analysis," *Phys. Rev. Fluids*, Vol. 3, 2018, p. 053902. https://doi.org/10.1103/PhysRevFluids.3.053902.

[53] Timme, S., "Global instability of wing shock buffet," 2018. arXiv: 1806.07299.

[54] Ohmichi, Y., Ishida, T., and Hashimoto, A., "Modal Decomposition Analysis of Three-Dimensional Transonic Buffet Phenomenon on a Swept Wing," *AIAA Journal*, Vol. 56, No. 10, 2018, pp. 3938–3950. https://doi.org/10.2514/1.J056855.

[55] Masini, L., Timme, S., and Peace, A. J., "Analysis of a civil aircraft wing transonic shock buffet experiment," *Journal of Fluid Mechanics*, Vol. 884, 2020, p. A1. https://doi.org/10.1017/jfm.2019.906.

[56] Giannetti, F., and Luchini, P., "Structural sensitivity of the first instability of the cylinder wake," *Journal of Fluid Mechanics*, Vol. 581, 2007, p. 167–197. https://doi.org/10.1017/S0022112007005654.

[57] Sipp, D., and Lebedev, A., "Global stability of base and mean flows: a general approach and its applications to cylinder and open cavity flows," *Journal of Fluid Mechanics*, Vol. 593, 2007, p. 333–358. https://doi.org/10.1017/S0022112007008907.

[58] Beran, P. S., Khot, N. S., Eastep, F. E., Snyder, R. D., and Zweber, J. V., "Numerical Analysis of Store-Induced Limit-Cycle Oscillation," *Journal of Aircraft*, Vol. 41, No. 6, 2004, pp. 1315–1326. https://doi.org/10.2514/1.404.